Microporous and Mesoporous Materials 328 (2021) 111488

Contents lists available at ScienceDirect

Microporous and Mesoporous Materials

journal homepage: www.elsevier.com/locate/micromeso

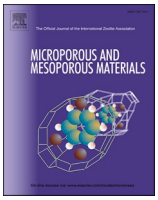

Synthesis of Cu(I) doped mesoporous carbon for selective capture of ethylene from reaction products of oxidative coupling of methane (OCM)

Dipendu Saha [a,*], Marisa Comroe [a], Rajamani Krishna [b]

[a] Department of Chemical Engineering, Widener University, One University Place, Chester, PA, 19013, USA
[b] Van't Hoff Institute for Molecular Sciences, University of Amsterdam, Science Park 904, 1098 XH, Amsterdam, the Netherlands

ARTICLE INFO

Keywords:
Porous carbon
Adsorption
Oxidative coupling of methane (OCM)
Ethylene recovery

ABSTRACT

There is a growing industrial interest in the recovery of ethylene from the gaseous products obtained in oxidative coupling of methane (OCM). The key challenge of employing OCM is the separation of ethylene from the product mixture that usually consists of ethylene, ethane, methane, carbon dioxide, carbon monoxide and hydrogen. In this work, we have synthesized Cu(I) doped mesoporous carbons as ethylene selective adsorbents to separate ethylene from the product mixture of OCM. The pristine mesoporous carbon was synthesized from resorcinol as carbon precursor and F127 as surfactant template. Cu(I) doping on mesoporous carbon was performed by CuCl as the precursor of Cu(I) with total Cu content of 0.3–3.3at.% in the resultant carbon. The structural identity of carbons was confirmed by pore textural properties, scanning electron microscopy (SEM), Energy dispersive X-ray (EDX), X-ray photoelectron spectroscopy (XPS) and X-ray diffraction (XRD). It was revealed that the selectivity towards ethylene is a function of Cu content of the mesoporous carbon indicating a possible π-complexation between ethylene and Cu(I). Pure component adsorption isotherms confirmed that ethylene adsorption is the highest followed by carbon dioxide, ethane, methane, carbon monoxide and hydrogen. IAST-based selectivity values for C_2H_4/C_2H_6, C_2H_4/CH_4, C_2H_4/CO_2, C_2H_4/CO and C_2H_4/H_2 were calculated as 8-4, 80-48, 22-4, 251-36, 7644-18120767, respectively. The isosteric heat of adsorption of ethylene was in the range of 54-26 kJ/mol and it was higher than that of the other gases. The adsorbent also demonstrated good cyclability of ethylene adsorption. Finally, the simulated dynamic breakthrough results for fixed bed adsorption column demonstrated a large interval between the breakthrough times of ethylene and other gases, confirming its separation. The overall results confirm that Cu(I)-doped mesoporous carbons have a high potential for ethylene separation from OCM gas mixtures.

1. Introduction

The separation of alkenes from alkanes and other gas mixtures is one of the key separation needs of the modern world [1]. Ethylene is one such high-demand alkene due to its role in the synthesis of polyethylene, which is the one of the most widely used plastics of modern world. For polymerization, the purity of ethylene must be greater than 99.95%. Besides, polymerization, ethylene is also used in oxy-fuel in metal cutting and welding, fruit ripening, refrigerating, anesthesia, car glass manufacturing, rubber extraction and many other specialty chemical synthesis [2]. Ethylene is one of the most highly produced industrial feedstocks around the world, the total amount exceeding 150 million tones every year [3]. Now-a-days, ethylene is mostly produced by catalytic cracking of naphtha and ethane [4]. As those sources are highly dependent on fossil fuel, the production of ethylene is generally not considered as sustainable.

Production of ethylene by the oxidative coupling of methane (OCM) may be regarded as a more sustainable approach to generate ethylene in industrial scale [5–7]. This is because methane is considered as the cleanest fossil fuel and as a bridge between the traditional fossil fuel and complete sustainability. Methane causes 23–85% of low emission of carbon [8]. Current availability of natural gas (methane) in many sectors and new technological development in the extraction of methane from shell gas, like hydraulic fracturing will increase in the usages of methane by 50% in 20 years [9,10]. A typical OCM reaction by which ethylene could be obtained from methane can be formulated as the following reaction scheme [5], [11–14].

* Corresponding author.
E-mail address: dsaha@widener.edu (D. Saha).

https://doi.org/10.1016/j.micromeso.2021.111488
Received 10 May 2021; Received in revised form 2 October 2021; Accepted 6 October 2021
Available online 13 October 2021

$$2CH_4 + O_2 \xrightarrow{Catalyst,\ 750-950\ ^\circ C} C_2H_4 + 2H_2O\ \Delta H^0 = -209.3\frac{KJ}{mol\ CH_4} \quad (1)$$

This exothermic reaction is carried over a heterogeneous catalyst which activates CH_4 to generate methyl free radical that couples in the gas phase to generate ethane (C_2H_6), which subsequently undergoes dehydrogenation to produce ethylene (C_2H_4) and hydrogen (H_2). However, at the same time, the non-selective methyl radical also reacts with oxygen to produce carbon dioxide (CO_2) and carbon monoxide (CO) which are considered as the byproducts of the reaction. Needless to say that unreacted methane and ethane also remain in the product mixture making the overall yield of C_2H_4 in the final product is very low. In a typical product mixture of OCM, the compositions of C_2H_4, C_2H_6, CH_4, H_2, CO_2 and CO are 6%, 4%, 72%, 11%, 5% and 2%, respectively [4]. The reactions by which the byproducts are synthesized are given below [5].

$$2CH_4 + \frac{1}{2}O_2 \rightarrow C_2H_6 + H_2O\ \Delta H^0 = 20.2\frac{kJ}{mol\ CH_4} \quad (2)$$

$$CH_4 + 2H_2O \rightarrow CO_2 + 2H_2 \Delta H^0 = 802.6\ \frac{kJ}{mol\ CH_4} \quad (3)$$

$$CH_4 + \frac{1}{2}O_2 \rightarrow CO + 2H_2\ \Delta H^0 = 36.0\ \frac{kJ}{mol\ CH_4} \quad (4)$$

Along with a few other drawbacks of OCM, like low methane to ethylene conversion, that hinders its successful industrial implementation, the separation or enrichment of C_2H_4 from the product stream is probably the most difficult obstacle of this process. The physical properties of the individual gases, including kinetic diameter, boiling point, dipole moment, quadruple moment and polarizability are listed in detail in the literature [4]. Owing to the very close physical properties of many of the product gas mixtures with each other, conventional separation processes, like distillation, absorption or scrubbing are not useful for this process. Owing to the high volume of methane in the product stream (around 72%), methane needs to recycle in the process to maximize the cost and carbon efficiency of the process [4]. Among all the hurdles of the separation of OCM gas mixtures, the challenging one is the separation of ethylene from ethane. Owing to a the small difference in the boiling point of ethylene and ethane in the cryogenic range, cryogenic distillation is the state-of-the-art technology to separate them, which are extremely extensive, hazardous and hence not sustainable. The presence of other gaseous components such as CO_2 makes the separation of OCM product gases even more challenging. Therefore, the purification of the product mixtures of the OCM process may be associated abnormally high energy input and capital investment that makes this process practically infeasible [4].

Compared to traditional separation processes, adsorption can be highly benign, sustainable and cost-effective process if a suitable adsorbent can be designed. Despite the similarities between the physical properties of the OCM product mixtures, the unique property of ethylene that can enable separation is the presence of an unsaturated double, or π bond. A few typical unsaturated metallic sites can attract the π bond of ethylene by so-called π complexation to selectively adsorb an unsaturated alkene like ethylene [15–18] in the product mixture. In the literature, it was demonstrated that a Metal-Organic Framework (MOF), Mn_2(*m-dobdc*) (where *m-dobdc*$^{4-}$: 4,6-dioxido-1,3-benzenedicarboxylate) was successful to separate the product mixtures of OCM reaction [4]. In past, we have demonstrated that Ag(I)-doped porous carbon can successfully separate light alkenes (ethylene and propylene) from its corresponding alkane (ethane and propane) [19]. In this report, we have synthesized Cu(I)-doped mesoporous carbon as an ethylene selective adsorbent and successfully implemented to separate ethylene from the product mixture of the OCM reaction.

2. Experimental

2.1. Synthesis of Cu(I)-doped mesoporous carbons

The first step in the fabrication Cu(I)-doped mesoporous carbon is the synthesis of the pristine mesoporous carbon, similarly to our previous publications [20–22]. Typically, 5.0 g resorcinol (Sigma-Aldrich) as carbon precursor and 4.0 g Pluronic F127 (BASF) were dissolved in 25 mL mixture of 1:1 (v/v) DI water and Ethanol. After that, 0.45 mL 36% HCl was added and the mixture was stirred overnight. Then, 5 mL 37% formaldehyde was added in the mixture as the cross-linking agent and stirred for 24 h. After that, the white polymer was separated from the system and sprayed in a Petri dish for a 24 h curing. The polymer film was transferred into a porcelain boat and inserted in a Lindberg-Blue tube furnace for heating. The polymer was heated up to 400 °C with a 2 °C/min rate and then up to 1000 °C at the rate of 10 °C/min. After cooling to room temperature and the product was taken out of the furnace. All the heating and cooling operations were performed under N_2 gas flow.

The produced pristine mesoporous carbon (2 g) was mixed with 8 g of sodium thiosulfate ($Na_2S_2O_3$) in a commercial coffee grinder and the mixture was put in a porcelain boat. The porcelain boat was inserted in the same tube furnace and it was heated upto 800 °C at the ramp of rate of 10 °C/min and cooled down to room temperature under N_2 gas flow. After that it is taken out from the furnace and resultant product was washed several times with DI water until a completely clear wash solution was obtained with pH close to neutral. The carbon was filtered out and dried in oven at 80 °C. This sulfurized carbon was mixed different amounts of anhydrous CuCl (Sigma-Aldrich, freshly opened from ampule) and ground in a mortar and pestle for 45 min. After that, the mixture was inserted in the porcelain boat and heated in the tube furnace at 500 °C at a rate of 5 °C/min under N_2 gas flow and then cooled to room temperature. The resultant carbon was washed with DI water, filtered and dried in the same fashion. In these three batches of Cu(I) doping, 1.16 g, 1.10 g, and 1.2 g of sulfurized mesoporous carbons were mixed with 0.057 g, 0.107 g, 0.151 g CuCl and they are named as MC-Cu-1, MC-Cu-2 and MC-Cu-3, respectively. The schematic of synthesis of Cu(I) doped mesoporous carbon is shown in Fig. 1.

2.2. Materials characterizations

X-ray diffraction experiments were obtained in a Bruker D8 model A25 with a *CuKα* x-ray source. Scans were done at a step size of 0.05° and dwell time of 1s per step. Scanning electron microscopy (SEM) imaging and energy dispersive x-ray (EDX) were performed in a FEI Quanta 600 FEG Mark II Environmental Scanning Electron Microscope (ESEM). X-ray photoelectron spectroscopy (XPS) data were obtained in a Thermo-Fisher K- alpha instrument using an *AlKα* x-ray source (1486.7 eV) and with an overall resolution of 0.7 eV. Charge compensation was performed by using a combination of low energy electrons and ions. The pore textural properties including the BET surface area and the total pore volume were obtained by analyzing N_2 adsorption isotherms obtained 77 K. The pore size distribution was obtained by non-local density function (NLDFT) theory that was applied in N_2 adsorption isotherm at 77 K and CO_2 adsorption at 273 K. The narrower pore widths (less than 10 Å) were obtained from CO_2 adsorption isotherm whereas the larger pore widths (greater than 10 Å) were obtained from N_2 adsorption isotherms [23,24]. The isotherms were measured in a Quantachrome's Autosorb iQ-Any Gas instrument.

2.3. Adsorption experiments

All the gas adsorption isotherms were obtained in the same Autosorb iQ-Any Gas instrument at 298 K and pressure upto 760 torr. All the gases were of ultra-high purity (UHP) grade or higher. The temperature was maintained by an external chiller (Julabo). The kinetic data of the gases

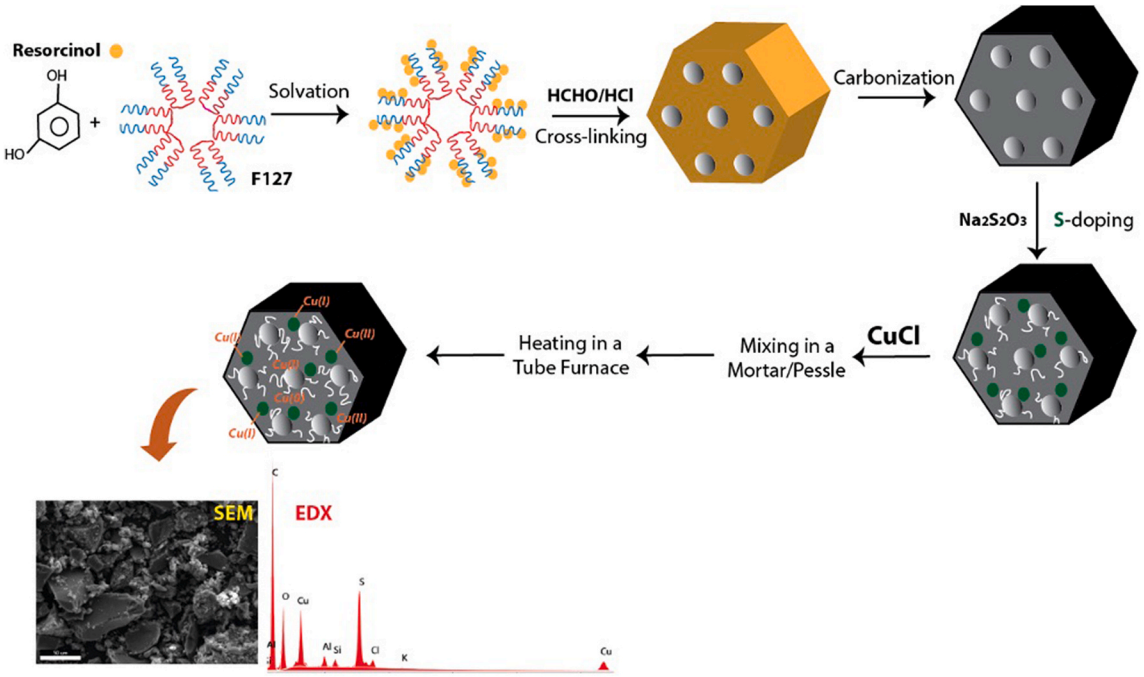

Fig. 1. Schematic of synthesis of Cu(I)-doped mesoporous carbon.

were obtained in the same instrument under vector dose mode. The continuous cycles of adsorption and desorption were measured under hysteresis mode.

3. Results and discussion

3.1. Materials characterizations

3.1.1. Electron microscopy

Scanning electron microscopic (SEM) images of MC-Cu-1, MC-Cu −2 and MC-Cu −3 are shown in Fig. 2(a–c). It is observed that the carbons have no specific shape or size. In general, particles in MC-Cu-1 and -3 have a similar size range of 2–12 μm. The particle size of MC-Cu-2 is much smaller, in the range of 0.25–1.3 μm. The energy dispersive X-ray (EDX) mapping for carbon (C–K), oxygen (O–K), sulfur (S–K), copper (Cu–K) and chlorine (Cl–K) of Cu-MC-2 are shown in Fig. 3(a–f). The corresponding information for MC-Cu-1 and MC-Cu-3 is shown in the supporting information (Figs. S1 and S2). From the mapping, it is clear that these atoms are distributed in the carbon matrix quite uniformly. EDX spectra, indicate that the total Cu contents of MC-Cu-1, MC-Cu-2 and MC-Cu-3 are 0.6 at.%, 3.3 at.% and 0.3 at.%, respectively. The total Cu content of MC-Cu-1 and MC-Cu-2 increased monotonically with increasing CuCl load (or the ratio of CuCl/sulfurized carbon) as mentioned in the experimental section, but it decreased rapidly with further increase in MC-Cu-3. Although such phenomenon may be regarded as counter-intuitive, further investigation of the overall sulfur content within the three adsorbents provide some answer. The sulfur content of MC-Cu-1 and MC-Cu-2 is quite high (4.8 and 4.3 at.% respectively), but quite low in MC-Cu-3 (0.4 at.%). As all the initial sulfurized carbons had the same sulfur content, it can be concluded that an excess amount of CuCl in the reaction phase does not increase the Cu loading of the resultant carbon. Instead, CuCl reacts with sulfur functionalities and gets removed from the system under the form of soluble salts, probably during washing. Pore textural properties studies, as will be seen, points to another major role for the excess CuCl precursor.

3.1.2. X-ray photoelectron spectroscopy (XPS)

In order to provide further light on the type of functionalities present in our adsorbent carbon material, X-ray photoelectron spectroscopy (XPS) was performed. The XPS results revealed that MC-Cu-2 has total carbon and copper contents of around 73.49 at.%. and 3.27 at.%, respectively. MC-Cu-2 also possesses O, S and Cl with percentages of 19.68, 3.28 and 0.29 at.%, respectively. The deconvolution results of Cu-2p and S-2p peaks are shown in Fig. 4. Similar deconvolution results for C-1s, O-1s and Cl-2p peaks are provided Fig. S3 of the supporting information. From the deconvolution of the S-2p peak, it was revealed that Cu–S bond is 0.23 at.%, whereas other sulfur functionalities are 3.05 at.%. It is obvious that, during thermal reaction, CuCl reacted with some sulfur functionalities present on the carbon surface and partly converted to Cu–S functionalities. The remaining S-functionalities were attributed to the pristine sulfur functionalities present at the carbon surface. From the Cu-2p peak deconvolution, it was also revealed that 2.51 at.% copper was present as Cu(II), whereas 0.76 at.% copper remained as Cu(I) or Cu(0). It is quite imperative to think that a large fraction of Cu(I) was oxidized to Cu(II) in the course of thermal reaction, whereas a smaller part remained as Cu(I). Since the diffraction peak of Cu(0) was not noticed in the XRD pattern (Fig. 5), possibly only Cu(I) was present in the amount of 0.76 at.%. Moreover, by the deconvolution of Cl-2p peak, it was revealed that 0.29 at.% Cu–Cl bond was present in the system that originated from the main the precursor of CuCl.

3.1.3. X-ray diffractions (XRD)

The X-ray diffraction (XRD) patterns of all the Cu(I)-doped carbons are shown in Fig. 5. In all the patterns, the broad peaks at around $2\theta \approx 24^{\circ}$ and 44° belonged to the residual (002) and (101) reflections of graphitic structures and can be observed in almost all porous carbons [25]. From XRD, different peaks of CuCl have been observed, at around 25°, 43° and 57°. In the course of reaction, most likely, some of the Cu(I) is converted to Cu(II), probably in the form of $CuCl_2$, CuO, CuS, $CuSO_4{\cdot}5H_2O$ and Cu(OH)Cl [26–29]. Those Cu(II) species have been identified as 2, 3, 5, 6 and 7, respectively and marked in the XRD plot. Besides CuCl, the possible Cu(I) species that have been identified as Cu_2O. It is also important to note that these peaks are weaker in MC-Cu-3 compared to two other carbons due to the smaller amount of copper present in them.

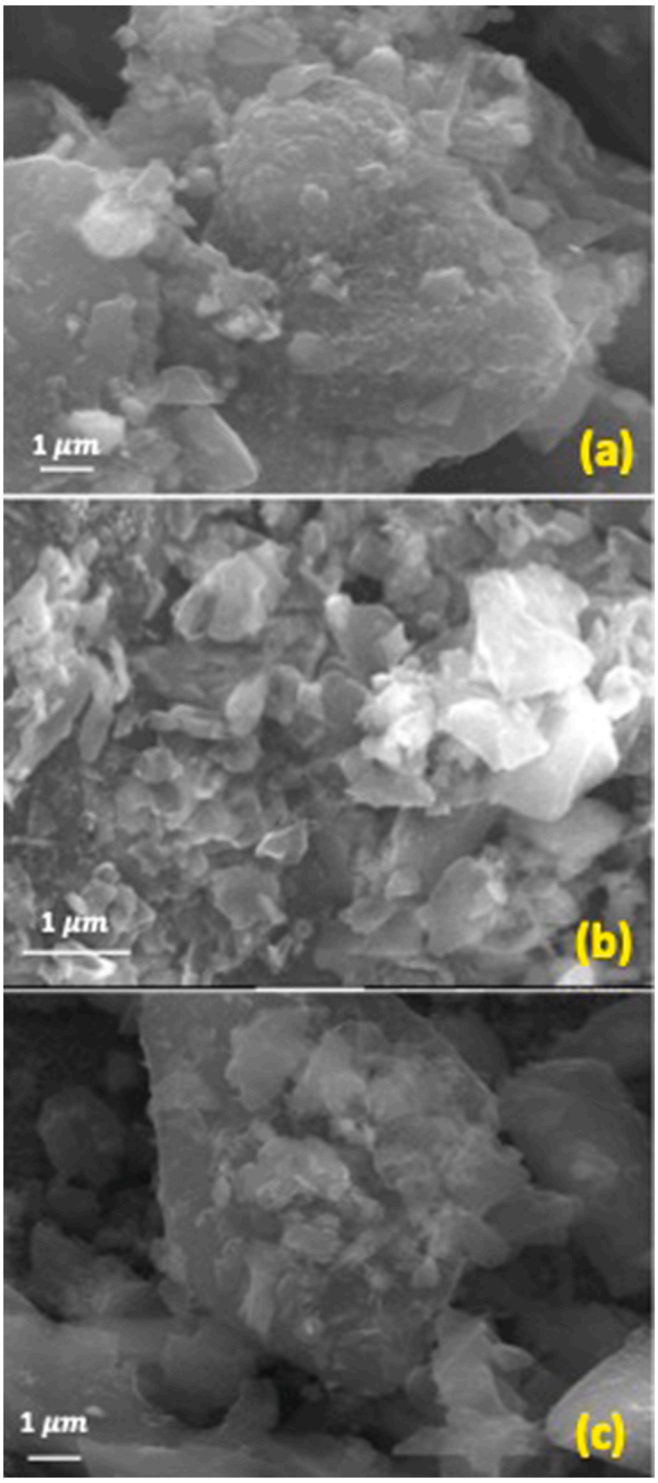

Fig. 2. Scanning electron microscopic image (SEM) of MC-Cu-1 (a), MC-Cu-2 (b) and MC-Cu-3 (c).

3.1.4. Pore textural properties

The BET surface area and total pore volume of all the carbons were obtained by analyzing N_2 adsorption isotherms at 77 K. The N_2 adsorption isotherms are shown in Fig. 6(a). All the isotherms are of type- IV according to IUPAC nomenclatures and the hysteresis loop signifies the presence of mesoporosity. The pore textural properties of the adsorbents are tabulated in detail in Table 1. The BET specific surface area (SSA) of MC-Cu-1, MC-Cu-2 and MC-Cu-3 are 320, 343 and 438 m^2/g, respectively. It is evident that BET SSA and pore volume increased with the increase in the dosing of CuCl in the reaction phase. The pore size distribution of all the three adsorbents is shown in Fig. 6(b) with the magnified view of narrow micropore distribution in the inset figure (Fig. S4, supporting information). The pore size distribution results were obtained from N_2 adsorption at 77 K and CO_2 adsorption at 273 K. As observed in the figure, all the carbons have a mesopore width in the range of 35–38 Å and a super micropore in the range of 15 Å. In the ultramicropore width region, the carbons have the pores in the widths in the range of 4.3 Å and 5.2 Å. MC-Cu-2 has an additional pore width of 6.2 Å. The narrowest pore present in 3.49 Å is probably not a true pore but a graphite layer spacing.

As mentioned in section 3.1.1, MC-Cu-3, which was synthesized with the highest loading of CuCl, manifests the lowest amount of total Cu, unlike the two other adsorbents. Such an anomaly can be explained with the hypothesis that additional CuCl in the reaction phase causes an excess reaction with the carbon and its functionalities, thereby lowering the Cu amount in the final product. This hypothesis can be strengthened by the unusually high surface area and porous nature of MC-Cu-3 compared to the two other carbon adsorbents. It becomes obvious that higher loading of CuCl acts more or less like an additional 'activating' agent reacting with the carbon matrix, and generating higher porosity instead of being a 'doping' agent, depositing Cu on the matrix. We therefore did not attempt to further increase the Cu loading. The relationship between the CuCl dose and the final Cu content and BET surface area is further exemplified in Fig. 7.

3.2. Pure-component adsorption of OCM gas components

Since the separation of ethylene from ethane is the challenging part of the separation, we made an initial attempt to measure the isotherms of pure ethylene and ethane in all the adsorbents and the results are shown in Fig. 8. As observed in the figure, MC-Cu-2 demonstrates the largest difference between the ethane adsorption and ethylene adsorption. MC-Cu-1 in comparison, only shows a smaller difference and while MC-Cu-3 indicates no difference. As observed in the same figure, the adsorbed amounts of both ethylene and ethane are highest for MC-Cu-3, which can be attributed to highest surface area and pore volume compared to the other adsorbents.

All the isotherms were modeled with Langmuir-Freundlich or Sips model, given by

$$q = q_{sat}\frac{bp^{\upsilon}}{1+bp^{\upsilon}} \tag{5}$$

where, q is the adsorbed amount (mmol/g), p is the pressure (Pa) and, q_{sat}, b and υ are constants. The value of those constants are given in the supporting information (table s1-S3).

In order to investigate the separation performance of an adsorbent based on the pure component gas adsorption isotherm data, it is a common practice to report the selectivity values based Ideally adsorbed solution theory (IAST) [30]. IAST-based selectivity component "1" (preferred component) over component "2" (non-preferred component) It is given by

$$\alpha_{1/2} = \frac{q_1/q_2}{p_1/p_2} \tag{6}$$

where q_1, q_2 are the molar loadings (units: mmol g^{-1}) in the adsorbed phase in equilibrium with a gas mixture with partial pressures p_1, p_2 in the bulk gas. The IAST-based selectivity of ethylene over ethane in an equimolar mixture for all the three adsorbents is shown in Fig. 9. As observed in the figure, MC-Cu-2 has the highest selectivity of ethylene over ethane, which are in the range of 8-4. MC-Cu-1 and MC-Cu-3 demonstrated very low selectivity that are only slightly higher than 1.0.

It needs to be noted that the selectivity values for ethylene are monotonically related to the Cu content of the adsorbents and increases from MC-Cu-3 to MC-Cu-2. The higher adsorption isotherms of an

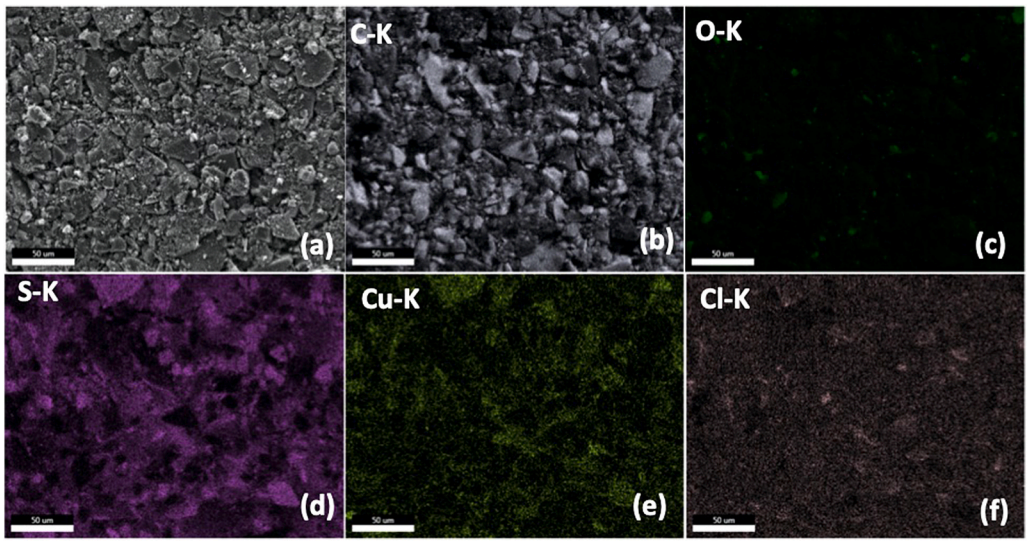

Fig. 3. SEM of MC-Cu-2 (a) and the corresponding K-shell EDX mapping for C (b), O (c), S(d), Cu (e) and Cl (f). Similar figures for Cu-MC-1 and Cu-MC-2 have been provided in the supporting information.

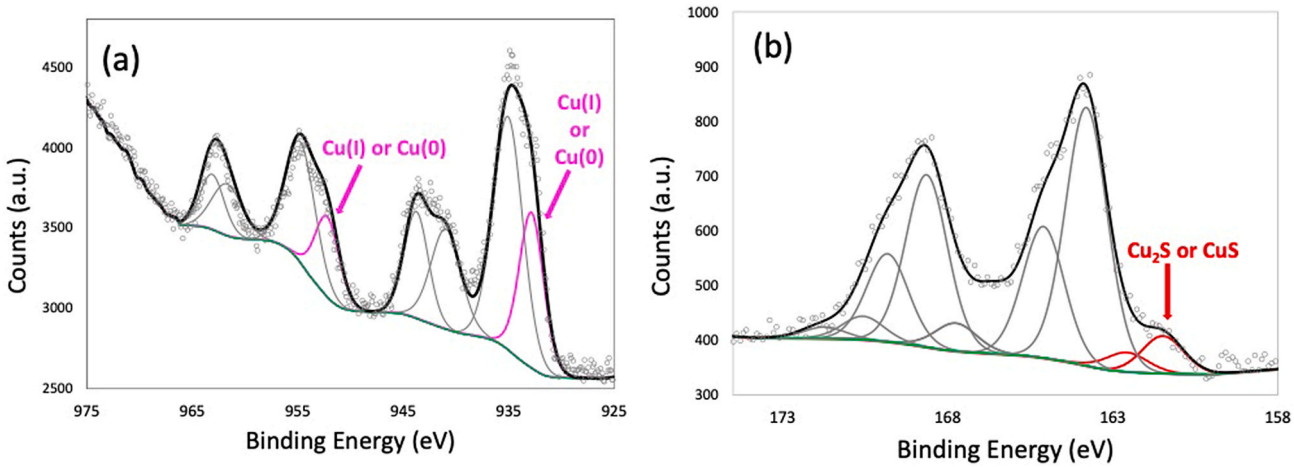

Fig. 4. X-ray photoelectron spectroscopy (XPS) results of the Cu-2p (a) and S-2p (b) for MC-Cu-2. Additional XPS spectra for C-1s, O-1s and Cl-2p are provided in the supporting information.

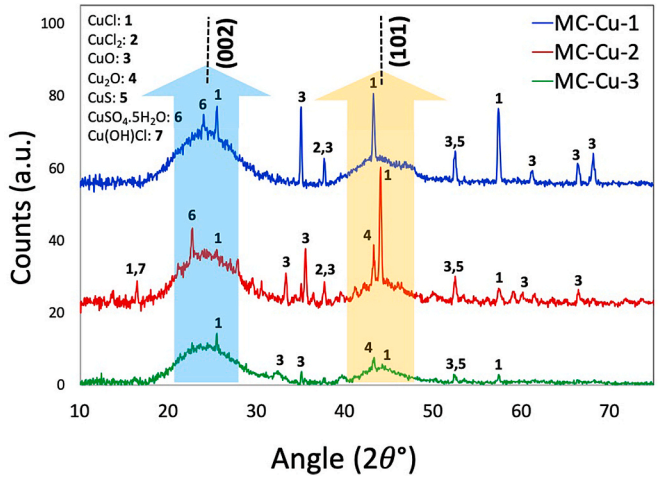

Fig. 5. X-ray diffraction (XRD) patterns of MC-Cu-1, MC-Cu-2 and MC-Cu-3.

alkene, like ethylene compared to that of an alkane, like ethane, can be explained by π complexation. π complexation is a type of selective chemical bond sharing between the π orbitals of olefins and partially vacant orbitals few cations, like Ag(I) or Cu(I) [31–34]. At the sufficient proximity of the olefin and Cu(I) ion, the partial overlap between π orbital of olefin and *s*- or *d*-orbital of Cu(I) will take place. The full π orbital of olefin overlaps with the empty *s* orbital of the Cu(I) and electron donation takes place from olefin towards Cu(I) ion. At the same time, the full d_{yz} orbital of the Cu(I) overlaps with π* antibonding orbital of olefin resulting in a backdonation of electrons from filled *d*-orbital towards π* antibonding orbital. Such a complexation partially loosens the C–C bond of olefins but the overall molecular entity of olefins remains completely intact [35]. Lowering of pressure or gentle heating of the system breaks down the complexation. The schematic of π complexation is shown in Fig. 10.

As MC-Cu-2 demonstrated the best separation efficiency of MC-Cu-2, we have selected it for the adsorption of all the gaseous components of OCM product mixture. The pure-component adsorption isotherms of C_2H_4, C_2H_6, CH_4, CO_2, CO and H_2 on MC-Cu-2 are shown in Fig. 11. As observed in this figure, MC-Cu-2 is an ethylene selective adsorbent with ethylene adsorbed amount is higher than that of any gas measured. CO_2

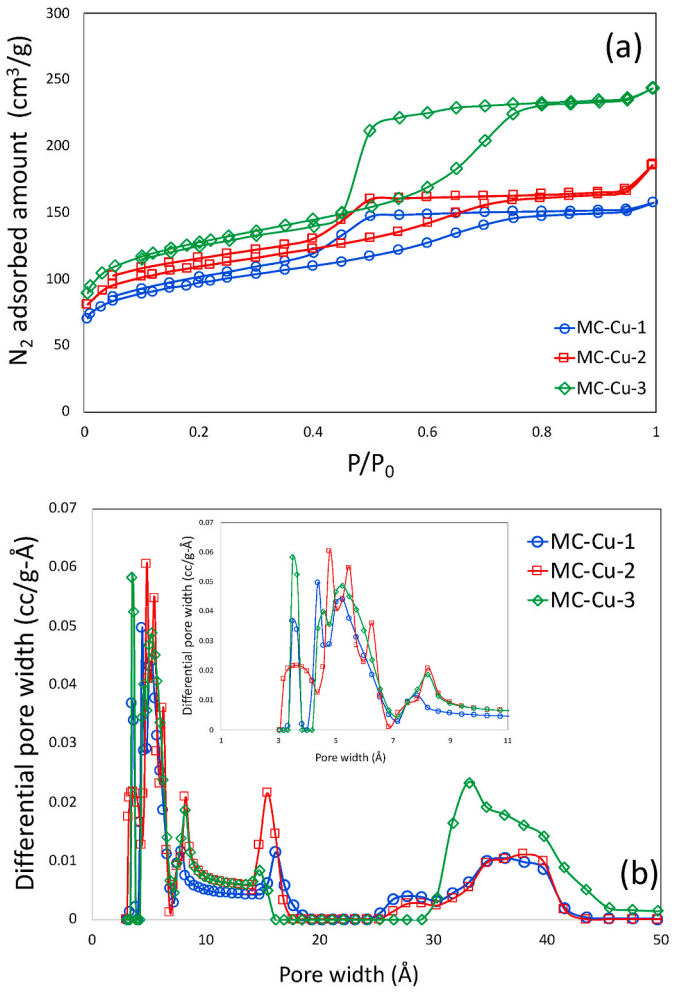

Fig. 6. N_2 adsorption-desorption results (a) and pore size distribution obtained by non-local density function theory (NLDFT) (b) of MC-Cu-1, MC-Cu-2 and MC-Cu-3.

Table 1
Pore Textural Properties of the adsorbents.

Adsorbents	BET SSA (m^2/g)	Micropore volume (cm^3/g)	Mesopore volume (cm^3/g)	Total Pore volume (cm^3/g)
MC-Cu-1	320	0.112	0.106	0.218
MC-Cu-2	343	0.137	0.110	0.247
MC-Cu-3	438	0.120	0.218	0.338

adsorbed amount is slightly higher than that of C_2H_6 followed by CH_4, CO and H_2. Like all other adsorbents, H_2 gas is always minimally adsorbed at the ambient temperature. All the adsorption isotherms were modeled by Sips isotherm according to equation (5). The values of model constants are given in the supporting information (Table S2). As there was no Cu(I) doped carbonaceous adsorbents were reported in literature, we have compared the adsorption capacity of C_2H_4 with Cu(I) functionalized MOFs [36], Cu^1@UiO-66-COOH and Cu^1@UiO-66-$(COOH)_2$. It was reported that the C_2H_4 uptake was in the range of 1.4–1.8 mmol/g at 298 K and 1 bar that are lower than that of MC-Cu-2, as observed in Fig. 11. Both of those MOFs also selective to C_2H_4 compared to that of C_2H_6. Another series of Cu bearing and ultra-microporous MOFs [37] demonstrated elevated C_2H_4 adsorbed amount of around 2.5 mmol/g, although those materials demonstrated lower selectivity of ethylene in presence of ethane and those are further elaborated in the following sections. A copper bearing MOF, Cu-MOF-74

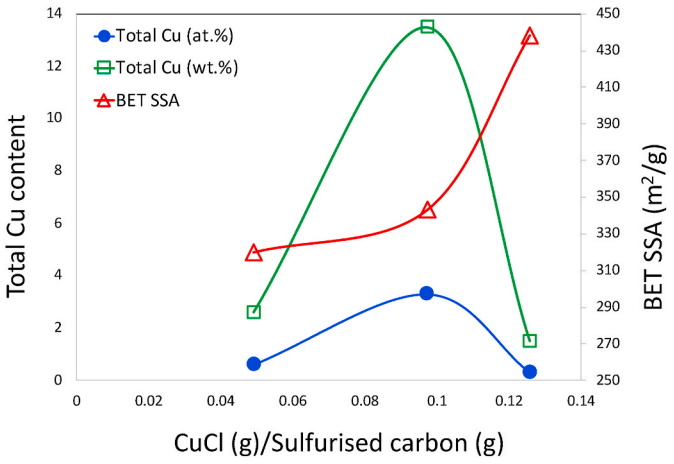

Fig. 7. Correlation of copper content and BET surface area with the CuCl in the synthesis phase.

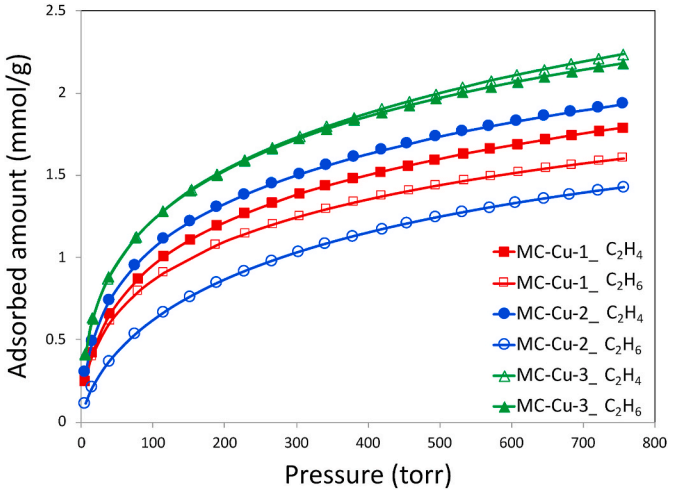

Fig. 8. C_2H_4 and C_2H_6 adsorption isotherms at 298 K on MC-Cu-1, MC-Cu-2 and MC-Cu-3.

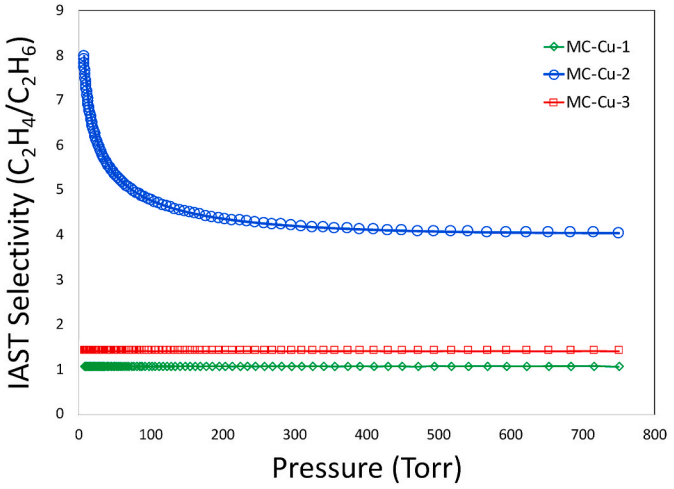

Fig. 9. IAST-based selectivity of C_2H_4/C_2H_6 in MC-Cu-1, MC-Cu-2 and MC-Cu-3.

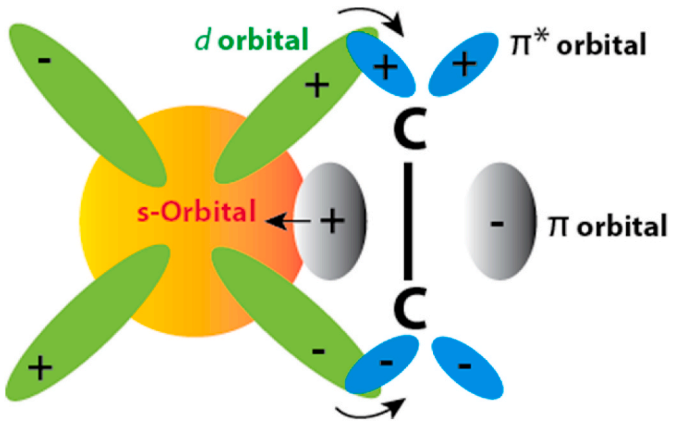

Fig. 10. Schematic of π complexation between metal ion (left) and olefin (right).

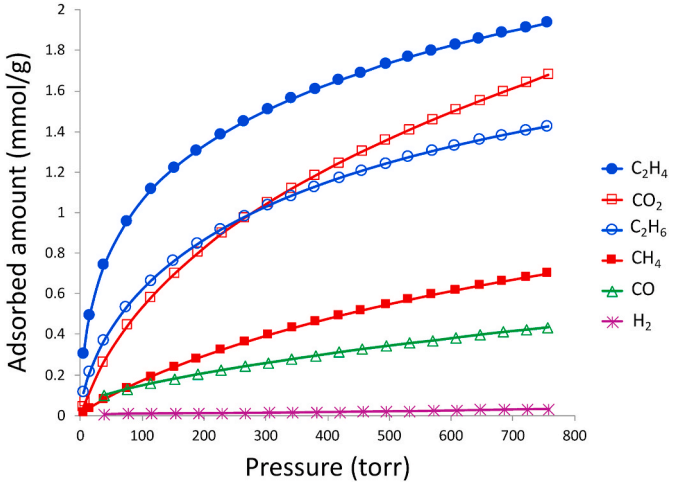

Fig. 11. Pure component adsorption isotherms of C_2H_4, C_2H_6, CH_4, CO_2, CO and H_2 at 298 K on MC-Cu-2.

demonstrated a high C_2H_4 uptake of ~4 mmol/g, but its selectivity compared to C_2H_6 was not reported [38]. Nonetheless, the only ethylene-selective MOFs[4] that are reported to successfully separate OCM mixture, M_2(m-dobdc) (M = Fe^{2+} and Mn^{2+}) have very high uptake capacity of ~7 mmol/g that is most likely caused by both high surface area and stronger interactions with the open metal sites.

The kinetics of adsorption of the C_2H_4, C_2H_6, CH_4, CO_2, and CO on MC-Cu-2 are shown in Fig. 12. It is observed that ethane and ethylene have similar kinetics and achieved the saturation level of adsorption at around 150 s. The kinetics of CO_2 was slightly faster whereas kinetics of CH_4 was slightly slower. The kinetics of CO was noisy owing to its low adsorption amount and fast kinetics. We did not report kinetics of H_2 as it has a very low adsorbed amount and kinetics was extremely noisy. The kinetic data can be modeled with the first-term approximation as [39–41].

$$\left(1-\frac{q_t}{q_\infty}\right)=\frac{6}{\pi^2}exp\left(\frac{-\pi^2 D_c t}{r_c^2}\right) \tag{7}$$

where, q_t is the adsorbed amount at time t, D_c is intra-crystalline diffusivity and r_c is the intracrystalline radius. For materials like porous carbon, the intracrystalline radius cannot be defined and therefore it is a common practice to report the diffusive time constant as $\frac{D_c}{r_c^2}$. The diffusive time constant can be calculated linear regression of t versus $ln\left(1-\frac{q_t}{q_\infty}\right)$ within the $\frac{q_t}{q_\infty}$ value of 75%–99%. The diffusive time constants for C_2H_4, C_2H_6, CH_4, CO_2 and CO are 0.142 s^{-1}, 0.143 s^{-1}, 0.129 s^{-1}, 0.181 s^{-1} and 0.132 s^{-1}, respectively.

Owing to the difficulty in performing binary gas adsorption, it is a common trend to perform the pure-component gas adsorption and report the IAST-based selectivity. IAST-based selectivity of ethylene with respect to other gases of OCM mixture, i.e., C_2H_4/C_2H_6, C_2H_4/CO_2, C_2H_4/CH_4, and C_2H_4/CO at the equimolar mixtures are shown in Fig. 13, while the selectivity for C_2H_4/H_2 are shown in the inset of the same figure. It is observed that selectivity of C_2H_4 with respect to CO_2 is very similar to that of C_2H_6, except selectivity of CO_2 is slightly higher at the lower pressure. Selectivity of C_2H_4 with respect to CH_4 is the highest among all the hydrocarbons followed by CO. Quite obviously, its selectivity to C_2H_4 with respect to H_2 is the highest ranging from 8400 to 18120767. The Cu bearing MOF, Cu^1@UiO-66-COOH was reported to have the similar selectivity of C_2H_4 with respect to C_2H_6 (~10), however, Cu^1@UiO-66-$(COOH)_2$ had a selectivity that is one of magnitude higher [36]. The other Cu-bearing MOF [37], $Cu(Qc)_2$ and $Cu(ina)_2$ demonstrated much lower C_2H_4/C_2H_6 selectivity of more than 3.5. Although Fe^{2+} and Mn^{2+} based MOF, M_2(m-dobdc) demonstrated higher C_2H_4/C_2H_6 selectivity of 10–20 in the course of separating OCM mixture [4], Ni^{2+}, Co^{2+}, Mg^{2+} and Zn^{2+} -based M_2(m-dobdc) demonstrated quite inferior selectivity in a different study [42]. The selectivity

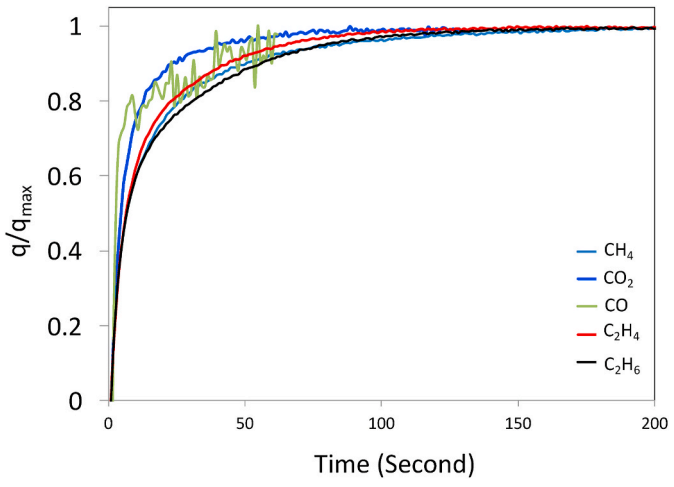

Fig. 12. Kinetics of C_2H_4, C_2H_6, CH_4, CO_2 and CO adsorption at 298 K on MC-Cu-2.

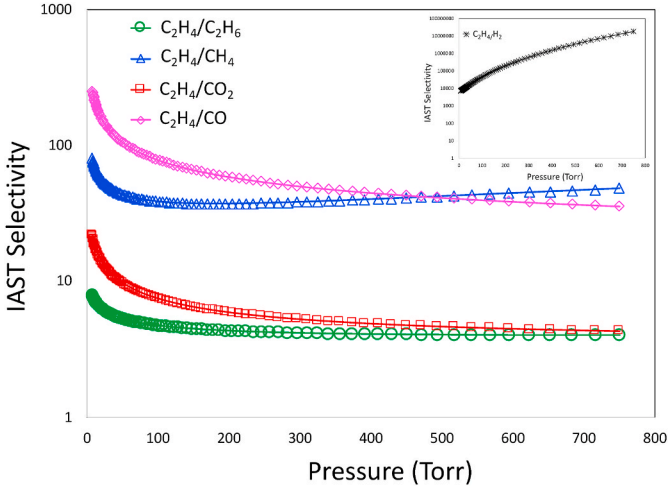

Fig. 13. IAST-based selectivity of C_2H_4/C_2H_6, C_2H_4/CH_4, C_2H_4/CO_2 and C_2H_4/CO on MC-Cu-2. The inset shows the IAST-based selectivity for C_2H_4/H_2.

of C_2H_4/CH_4, C_2H_4/CO_2 and C_2H_4/CO for Cu-MC-2 is lower compared to that of Fe^{2+} and Mn^{2+} based MOF, M_2(m-dobdc) [4].

The efficiency of an adsorbent is dependent on its constant working capacity in the repeating cycles of adsorption and desorption. The working capacity may be defined as the difference between the adsorbed amount at the pressure of 1 bar during adsorption cycle and 0.1 bar during consequent desorption cycle [38,43]. In order to study the working capacity of C_2H_4 on Cu-MC-2, we have performed 8 continuing cycles of adsorption and desorption of C_2H_4 at the temperature of 298 K. The results are shown in Fig. 14. It was observed that Cu-MC-2 maintained a fairly constant working capacity throughout all the cycles with a standard deviation not more than 2.7%.

Isosteric heat of adsorption (ΔH) can be calculated by the Van't Hoff equation, given by

$$\frac{\Delta H}{RT^2} = -\left(\frac{\partial \ln P}{\partial T}\right)_q \tag{8}$$

where ΔH is the isosteric heat of adsorption, T is the temperature, P is pressure and q is the adsorbed amount. An integration of Van't Hoff equation yields to

$$\frac{\Delta H}{RT} = \ln P + C \tag{9}$$

where, C is the constant of integration. The isosteric heat of adsorption (ΔH) can be calculated from the linear regression of $ln\ P$ versus $1/T$. The isosteric heat of adsorption values were calculated from the pure component isotherms at 273 K, 298 K and 318 K and as a function of adsorbed amount. The heat of adsorption for C_2H_4, C_2H_6, CH_4, CO_2 and CO are provided in Fig. 15. It is observed that C_2H_4 has the highest absolute heat adsorption values of 54-26 kJ/mol within the adsorbed amount of 0.16–1.62 mmol/g. Ethane has the lower heat of adsorption compared to that of ethylene followed by other gases. Higher heat of adsorption of C_2H_4 compared to other gases confirmed its affinity-based adsorption possibly by π -complexation and the better selectivity of C_2H_4 compared to other gases. In this regard, it needs to be emphasized that the heat of adsorption of C_2H_4 is higher compared to that of both C_2H_4 and C_2H_6 in other ethane selective carbonaceous adsorbents, including, fructose derived porous carbon [44], carbonized polydopamine adsorbent [45] and glucosamine-derived porous carbon [46]. The reported heat of adsorption [36] of C_2H_4 in Cu^1@UiO-66-COOH was lower than that of Cu-MC-2, but it is higher for Cu^1@UiO-66-$(COOH)_2$ at the elevated loading, which supports its better selectivity for C_2H_4 at the higher pressure. It needs to be noted that the heat of adsorption in these

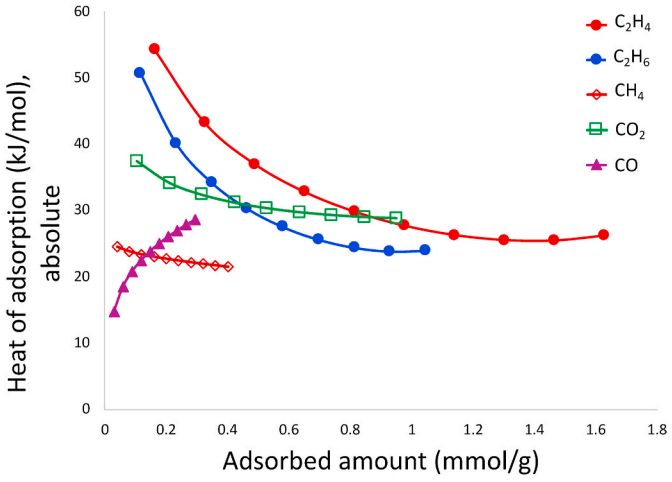

Fig. 15. Isosteric heat of adsorption of C_2H_4, C_2H_6, CH_4, CO_2 and CO on MC-Cu-2.

MOFs demonstrated an unusual linear profile that may signify an energetically heterogeneous surface. The heat of adsorption of MC-Cu-2 is also higher than another Cu bearing MOF [47], DUT-8(Cu), but it is selective to C_2H_6.

In order to understand the separation performance of the respective adsorbent in a fixed bed adsorption column, the transient breakthrough response should be studied. Due to the difficulty in measuring the experimental breakthrough response for a large number of gaseous components owing to the high instrument needs, it is a common practice to simulate the breakthrough response of the fixed bed adsorption column from the isotherm and selectivity data. In our study, we have simulated a fixed bed adsorber containing MC-Cu-2 as the adsorbent along with a six-component feed mixture consisting of C_2H_4, C_2H_6, CO, CH_4, H_2, CO_2 in ratio of 6, 4, 2, 72, 11 and 5%, respectively [4]. The operating conditions were 200 kPa pressure and 298 K temperature. The breakthrough simulations were carried out using in-house custom-built code methodology described in the previous publications [48–51]. For the breakthrough simulations, the following parameter values were used: length of packed bed, $L = 0.3$ m; voidage of packed bed, $\varepsilon = 0.4$; superficial gas velocity at inlet, $u = 0.04$ m/s.

Fig. 16 shows the simulated breakthrough plot. The x-axis of the plot is defined as the dimensionless time, $\tau = \frac{tu}{L\varepsilon}$, which is calculated by dividing the actual time, t, by the characteristic time, $\frac{L\varepsilon}{u}$. The sequence of breakthroughs is H_2, CO, CH_4, CO_2, C_2H_6 and C_2H_4. Particularly

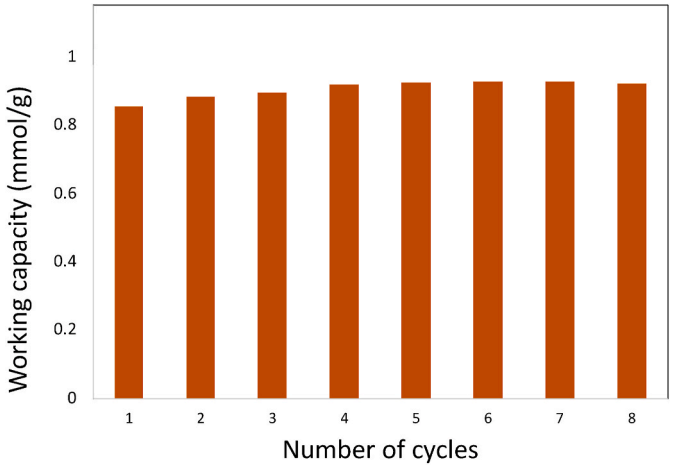

Fig. 14. Cyclability C_2H_4 adsorption on MC-Cu-2. The working capacity was calculated between 1 bar (adsorption pressure) and 0.1 bar (desorption pressure) at 298 K.

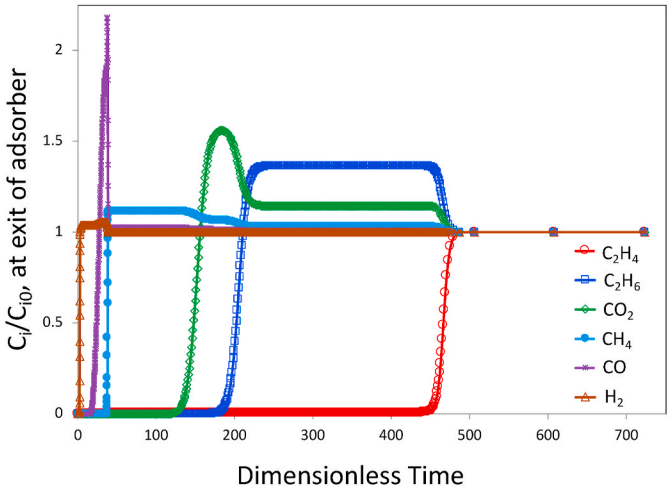

Fig. 16. Simulated fixed bed column breakthrough results on MC-Cu-2.

noteworthy is the large time interval between the breakthroughs of C_2H_6 and C_2H_4. It is evident that MC-Cu-2 is eminently suitable for use in the OCM process scheme that is illustrated in literature [52].

4. Conclusions

In this research, we have successfully synthesized Cu(I)doped mesoporous carbon from resorcinol as carbon precursor and CuCl as copper precursor. The material characterization confirmed the presence of Cu (I) species in the adsorbents. The BET surface area of the Cu(I) doped mesoporous carbons were in the range of 320–438 m^2/g. It is observed that the selectivity toward ethylene increases with increasing Cu content and this trend indicates the possible interaction of Cu(I) species with π bond of olefin. The adsorbent with 3.3 at.% of total copper content demonstrated the best selectivity towards ethylene and manifested itself as the ethylene selective adsorbent in the presence of an oxidative coupling of methane (OCM) product mixture, consisting of six gases including ethylene, ethane, methane, carbon dioxide, carbon monoxide and hydrogen. Calculation of IAST based selectivities also confirmed the selectivity of this adsorbent towards ethylene compared to the five other gases present in the system. Finally, simulations of transient breakthrough response from a fixed bed adsorption column containing this adsorbent demonstrated large time interval between ethylene and other gases. The overall results suggest that the Cu(I) doped mesoporous carbon can be a potential candidate to separate the product gas mixtures in the OCM reaction.

Declaration of competing interest

The authors declare that they have no known competing financial interests or personal relationships that could have appeared to influence the work reported in this paper.

Acknowledgement

This work was funded by American Chemical Society sponsored Petroleum Research Fund (ACS-PRF) with grant no. 59667-UR10 (PI: D. Saha).

Appendix A. Supplementary data

Supplementary data to this article can be found online at https://doi.org/10.1016/j.micromeso.2021.111488.

References

[1] D.S. Sholl, R.P. Lively, Seven chemical separations to change the world, Nature 352 (2018) 435–437.
[2] EL, Ethylene | Linde Gas, Linde Worldwide, 2020.
[3] R.B. Eldridge, Olefin/paraffin separation technology: a review, Ind. Eng. Chem. Res. 32 (1993) 2208–2212.
[4] J. Bachman, D.A. Reed, M.T. Kapelewski, G. Chachra, D. Jonnavittula, G. Radaelli, J.R. Long, Enabling alternative ethylene production through its selective adsorption in the metal–organic framework Mn (m-dobdc), Energy Environ. Sci. 11 (2018) 2423—2431.
[5] A. Cruellas, J.J. Bakker, M. van Sint Annaland, J.A. Medrano, F. Gallucci, Techno-economic analysis of oxidative coupling of methane: current state of the art and future perspectives, Energy Convers. Manag. 198 (2019) 111789.
[6] J. Ohyama, S. Nishimura, K. Takahashi, Data driven determination of reaction conditions in oxidative coupling of methane via machine learning, ChemCatChem 11 (2019) 4307–4313.
[7] V.O. Igenegbai, R. Almallahi, R.J. Meyer, S. Linic, Oxidative coupling of methane over hybrid membrane/catalyst active centers: chemical requirements for prolonged lifetime, ACS Energy Lett 4 (6) (2019) 1465–1470.
[8] I.A.A.C. Esteves, M.S.S. Lopes, P.M.C. Nunes, J.P.B. Mota, Adsorption of natural gas and biogas components on activated carbon, Separ. Purif. Technol. 62 (2008) 281–296.
[9] D. Saha, T. Fieback, B. Tom, Characteristics of methane adsorption in micro-mesoporous carbons at low and ultra-high pressure, Energy Technol. 4 (11) (2016) 1392–1400.
[10] S. Cavenati, C.A. Grande, A.E. Rodrigues, Adsorption equilibrium of methane, carbon dioxide, and nitrogen on zeolite 13X at high pressures, J. Chem. Eng. Data 49 (2004) 1095–1101.
[11] G. Olah, A. Molnar, Hydrocarbon Chemistry, John Wiley & Sons, New York, 2003.
[12] J.H. Lunsford, The catalytic coupling of methane, Angew. Chem. Int. Ed. Engl. 34 (1995) 970–980.
[13] B. Beck, V. Fleischer, S. Arndt, M.G. Hevia, A. Urakawa, P. Hugo, R. Schomacker, Oxidative coupling of methane- A complex surface/gas phase mechanism with strong impact on the reaction engineering, Catal. Today 228 (2014) 212–218.
[14] K. Otsuka, K. Jinno, A. Morikawa, Active and selective catalysts for the synthesis of C2H4 and C2H6 via oxidative coupling of methane, J. Catal. 100 (1986) 353–359.
[15] R.T. Yang, Gas Separation by Adsorption Processes, Imperial College Press, 1997.
[16] M. Herberhold, Metal Pi-Complexes: Part II: Specific Aspects, Elsevier, New York, 1974.
[17] D.J. Safarik, R.B. Eldridge, Olefin/paraffin separations by reactive absorption: a review, Ind. Eng. Chem. Res. 37 (1998) 2571–2581.
[18] B. Li, Y. Zhang, R. Krishna, K. Yao, Y. Han, Z. Wu, D. Ma, Z. Shi, T. Pham, B. Space, J. Liu, P.K. Thallapally, J. Liu, M. Chrzanowski, S. Ma, Introduction of π-complexation into porous aromatic framework for highly selective adsorption of ethylene over ethane, J. Am. Chem. Soc. 136 (2014) 8654–8660.
[19] D. Saha, B. Toof, R. Krishna, G. Orkoulas, P. Gismondi, R. Thorpe, M. Comroe, Separation of ethane-ethylene and propane-propylene by Ag(I) doped and sulfurized microporous carbon, Microporous Mesoporous Mater. 299 (2020) 110099.
[20] D. Saha, S. Barakat, S. Van Bramer, K.A. Nelson, D.K. Hensley, J. Chen, Non-competitive and competitive adsorption of heavy metals in sulfur-functionalized ordered mesoporous carbon, ACS Appl. Mater. Interfaces 8 (2016) 34132–34142.
[21] C.E. Unsworth, C.-C. Kuo, A. Kuzmin, S. Khalid, D. Saha, Adsorption of rare-earth elements in DNA functionalized mesoporous carbon, ACS Appl. Mater. Interfaces 12 (2020) 43180–43190.
[22] D. Saha, C.P. Richards, R.G. Haines, N.D. D'Alessandro, M.J. Kienbaum, C. A. Griffaton, Competitive adsorption of lead in sulfur and iron dual-doped mesoporous carbons, Molecules 25 (2019) 403.
[23] D. Saha, H.A. Grappe, Adsorption properties of activated carbon fibers, in: J. Y. Chen (Ed.), Activated Carbon Fiber and Textiles, Elsevier, Amsterdam, 2017, pp. 143–165.
[24] D. Saha, B. Tom, T.M. Fieback, Characteristics of methane adsorption in micro-mesoporous carbons in low and ultra-high pressure, Energy Technol. 4 (2016) 1392–1400.
[25] D. Saha, C.I. Contescu, N.C. Gallego, Tetrahydrofuran induced K and Li doping on to polyfurfuryl alcohol derived activated carbon: influence in microstructure and hydrogen sorption properties, Langmuir 28 (2012) 5669–5677.
[26] G.D. Marin, Z. Wang, G.F. Naterer, K. Gabriel, X-ray diffraction study of multiphase reverse reaction with molten CuCl and oxygen, Thermochim. Acta 524 (2011) 109–116.
[27] Q. Li, M. Shao, G. Yu, J. Wu, F. Li, Y. Qian, A solvent-reduction approach to tetrapod-like copper(I) chloride crystallites, J. Mater. Chem. 13 (2003) 424–427.
[28] H. Kokes, M.H. Morcali, E. Acma, Dissolution of copper and iron from malachite ore and precipitation of copper sulfate pentahydrate by chemical process, Eng. Sci. Technol. 17 (2014) 39–44.
[29] Z. Li, L. Mi, W. Chen, H. Hou, C. Liu, H. Wang, Z. Zheng, C. Shen, Three-dimensional CuS hierarchical architectures as recyclable catalysts for dye decolorization, CrystEngComm 14 (2012) 3965–3971.
[30] A.L. Myers, J.M. Prausnitz, Thermodynamics of mixed gas adsorption, AIChE J. 11 (1965) 121–127.
[31] R.T. Yang, Gas Separation by Adsorption Processes, Imperial College Press, 1987.
[32] M. Herberhold, Metal Pi-Complexes: Part II: Specific Aspects, Elsevier, New York, 1974.
[33] D.J. Safarik, R.B. Eldridge, Olefin/paraffin separations by reactive absorption: a review, Ind. Eng. Chem. Res. 37 (1998) 2571–2581.
[34] B. Li, Y. Zhang, R. Krishna, K. Yao, Y. Han, Z. Wu, D. Ma, Z. Shi, T. Pham, B. Space, J. Liu, P.K. Thallapally, J. Liu, M. Chrzanowski, S. Ma, Introduction of π-complexation into porous aromatic framework for highly selective adsorption of ethylene over ethane, J. Am. Chem. Soc. 136 (2014) 8654–8660.
[35] H.Y. Huang, J. Padin, R.T. Yang, Comparison of pi-complexations of ethylene and Carbon monoxide with Cu+ and Ag+, Ind. Eng. Chem. Res. 38 (1999) 2720–2725.
[36] L. Zhang, L. Li, E. Hu, L. Yang, K. Shao, L. Yao, K. Jiang, Y. Cui, Y. Yang, B. Li, B. Chen, G. Qian, Boosting ethylene/ethane separation within copper(I)-Chelated metal-organic frameworks through Tailor-made aperture and specific pi-complexation, Adv. Sci. 7 (2020) 1901918.
[37] R.-B. Lin, H. Wu, L. Li, X.-L. Tang, Z. Li, J. Gao, H. Cui, W. Zhou, B. Chen, Boosting ethane/ethylene separation within isoreticular ultramicroporous metal-organic frameworks, J. Am. Chem. Soc. 140 (40) (2018) 12940–12946.
[38] Y. Liao, L. Zhang, M.H. Weston, W. Morris, J.T. Hupp, O.K. Farha, Tuning ethylene gas adsorption via metal node modulation: Cu-MOF-74 for a high ethylene deliverable capacity, Chem. Commun. 53 (2017) 9376—9379.
[39] D.M. Ruthven, Principles and Adsorption and Adsorption Processes, 1984. New York.
[40] D. Saha, Z. Wei, S. Deng, Equilibrium, kinetics and enthalpy of hydrogen adsorption in MOF-177, Int. J. Hydrogen Energy 33 (2008) 7479–7488.
[41] D. Saha, S. Deng, Characteristics of ammonia adsorption on activated alumina, J. Chem. Eng. Data 55 (2010) 5587–5593.
[42] S.J. Geier, J.A. Mason, E.D. Bloch, W.L. Queen, M.R. Hudson, C.M. Brown, J. R. Long, Selective adsorption of ethylene over ethane and propylene over propane in the metal-organic frameworks M2(dobdc) (M = Mg, Mn, Fe, Co, Ni, Zn), Chem. Sci. 4 (2013) 2054–2061.

[43] D. Saha, G. Orkoulas, S.E. Van Bramer, H.-C. Ho, J. Chen, D.K. Hensley, CO2 capture in lignin-derived and nitrogen-doped hierarchical porous carbon, Carbon 121 (2017) 257–266.
[44] H. Xiao, Y. Wu, X. Wang, J. Peng, Q. Xia, Z. Li, A novel fructose-based adsorbent with high capacity and its ethane-selective adsorption property, J. Solid State Chem. 268 (2018) 190–197.
[45] X. Wang, Y. Wu, X. Zhou, J. Xiao, Q. Xia, H. Wang, Z. Li, Novel C-PDA adsorbents with high uptake and preferential adsorption of ethane over ethylene, Chem. Eng. Sci. 155 (2016) 338–347.
[46] X. Wang, Y. Wu, J. Peng, Y. Wu, J. Xiao, Q. Xia, Z. Li, Novel glucosamine-based carbon adsorbents with high capacity and its enhanced mechanism of preferential adsorption of C2H6 over C2H4, Chem. Eng. J. 358 (2019) 1114–1125.
[47] K.H. Cho, J.W. Yoon, J.H. Lee, J.C. Kim, K. Kim, U.-H. Lee, S.K. Kwak, J.-S. Chang, Effect of framework rigidity in metal-organic frameworks for adsorptive separation of ethane/ethylene, Microporous Mesoporous Mater. 307 (2020) 110473.
[48] R. Krishna, The Maxwell-Stefan description of mixture diffusion in nanoporous crystalline materials, Microporous Mesoporous Mater. 185 (2014) 30–50.
[49] R. Krishna, Methodologies for evaluation of metal-organic frameworks in separation applications, RSC Adv. 5 (2015) 52269–52295.
[50] R. Krishna, Screening metal-organic frameworks for mixture separations in fixed-bed adsorbers using a combined selectivity/capacity metric, RSC Adv. 7 (2017) 35724–35737.
[51] R. Krishna, Methodologies for screening and selection of crystalline microporous materials in mixture separations, Separ. Purif. Technol. 194 (2018) 281–300.
[52] I. van Zandvoort, E.-J. Ras, R. de Graaf, R. Krishna, Using transient breakthrough experiments for screening of adsorbents for separation of C2H4/CO2 mixtures, Separ. Purif. Technol. 241 (2020) 116706.

Supporting information

Synthesis of Cu(I) Doped Mesoporous Carbon as Ethylene Selective Adsorbent: Role in Separation of Gas-Mixtures in Oxidative Coupling Reaction of Methane (OCM)

Dipendu Saha, Marisa Comroe, Rajamani Krishna,

Table S1. Sips fit parameters for C_2H_4, and C_2H_6 in MC-Cu-1 at 298 K.

	q_{sat} mol kg^{-1}	b Pa$^{-\nu}$	ν dimensionless
C_2H_4	3	2.595E-03	0.55
C_2H_6	3	2.142E-03	0.55

Table S2. Langmuir-Freundlich fit parameters for C_2H_4, C_2H_6, CO, CH_4, H_2, and CO_2 in MC-Cu-2at 298 K.

	q_{sat} mol kg^{-1}	b $Pa^{-\nu}$	ν dimensionless
C_2H_4	3.5	3.090E-03	0.52
C_2H_6	2.3	4.938E-04	0.7
CO	3.6	1.200E-06	1
CH_4	1.2	1.300E-05	1
H_2	0.3	1.200E-06	1
CO_2	2.4	2.084E-05	1

Table S3. Sips fit parameters for C_2H_4, and C_2H_6 in MC-Cu -3 at 298 K.

	q_{sat} mol kg^{-1}	b $Pa^{-\nu}$	ν dimensionless
C_2H_4	3.8	4.365E-03	0.5
C_2H_6	3.8	4.208E-03	0.5

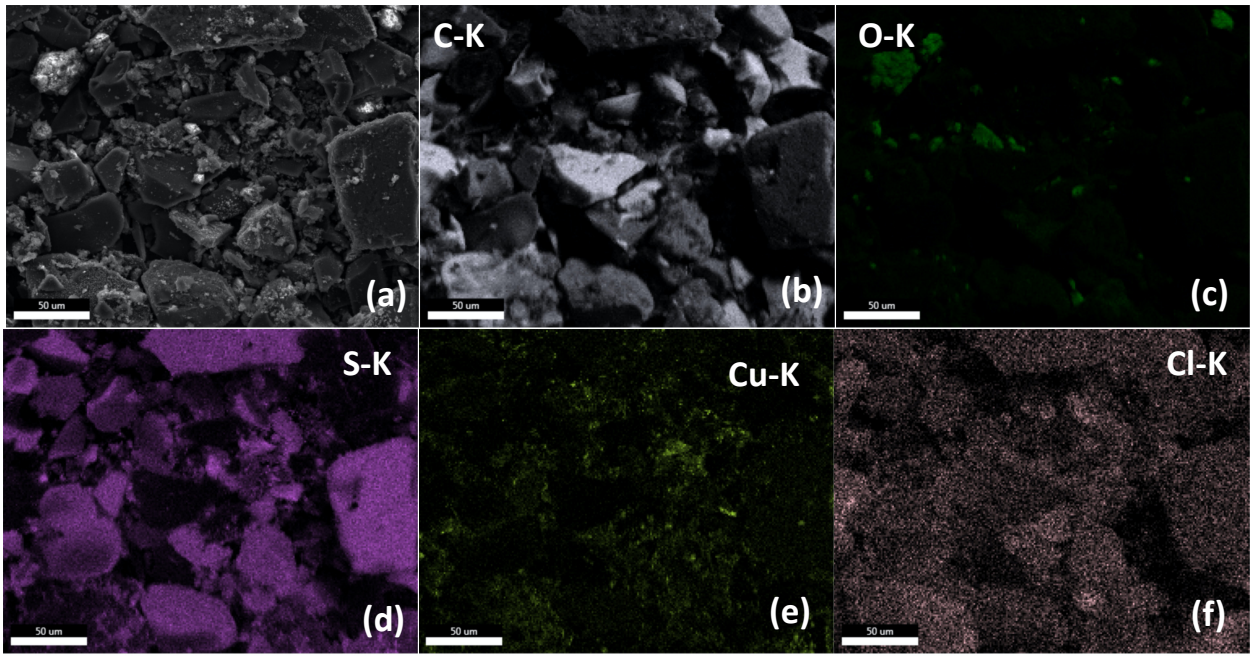

Figure S1. SEM of MC-Cu-1 (a) and the corresponding K-shell EDX mapping for C (b), O (c), S(d), Cu (e) and Cl (f)

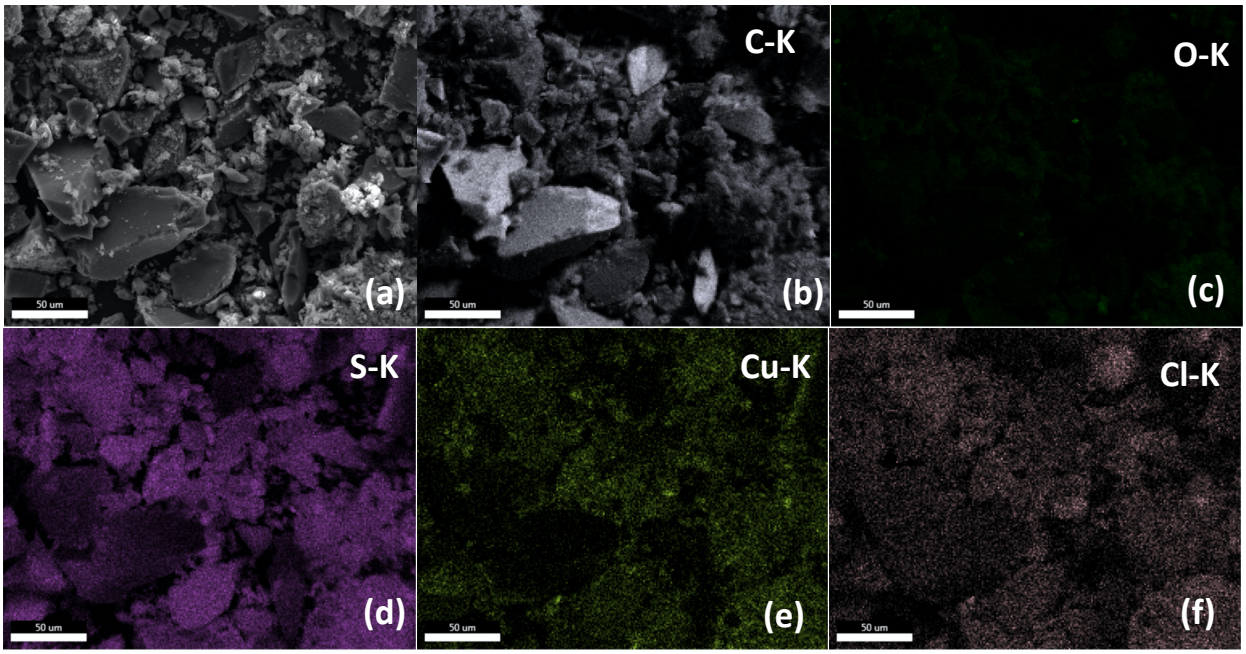

Figure S2. SEM of MC-Cu-3 (a) and the corresponding K-shell EDX mapping for C (b), O (c), S(d), Cu (e) and Cl (f)

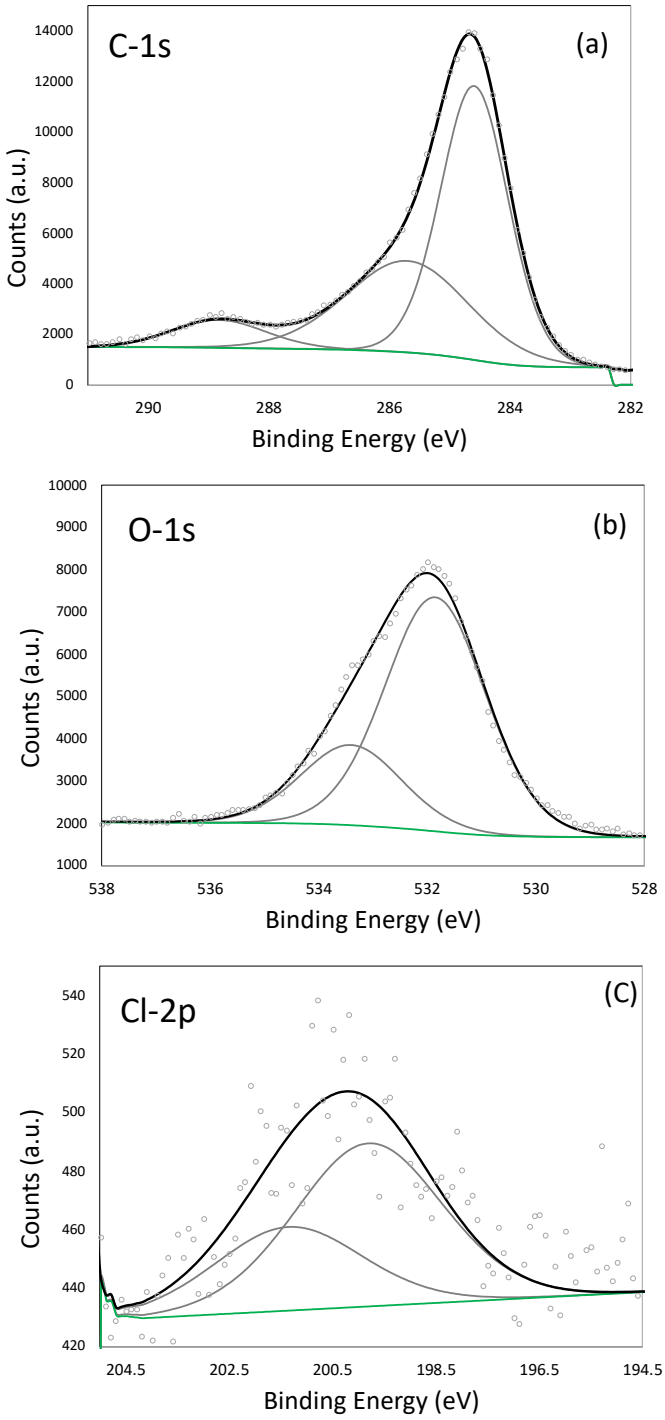

Figure S3. Core levels measured in XPS for MC-Cu-2 and peak fitting scheme: C-1s (a), O-1s (b) and Cl-2p (c) . C 1s and O 1s, possessing too many overlapping components and a complex structure, the fits presented are only use for total content estimation and not for chemical characterization.

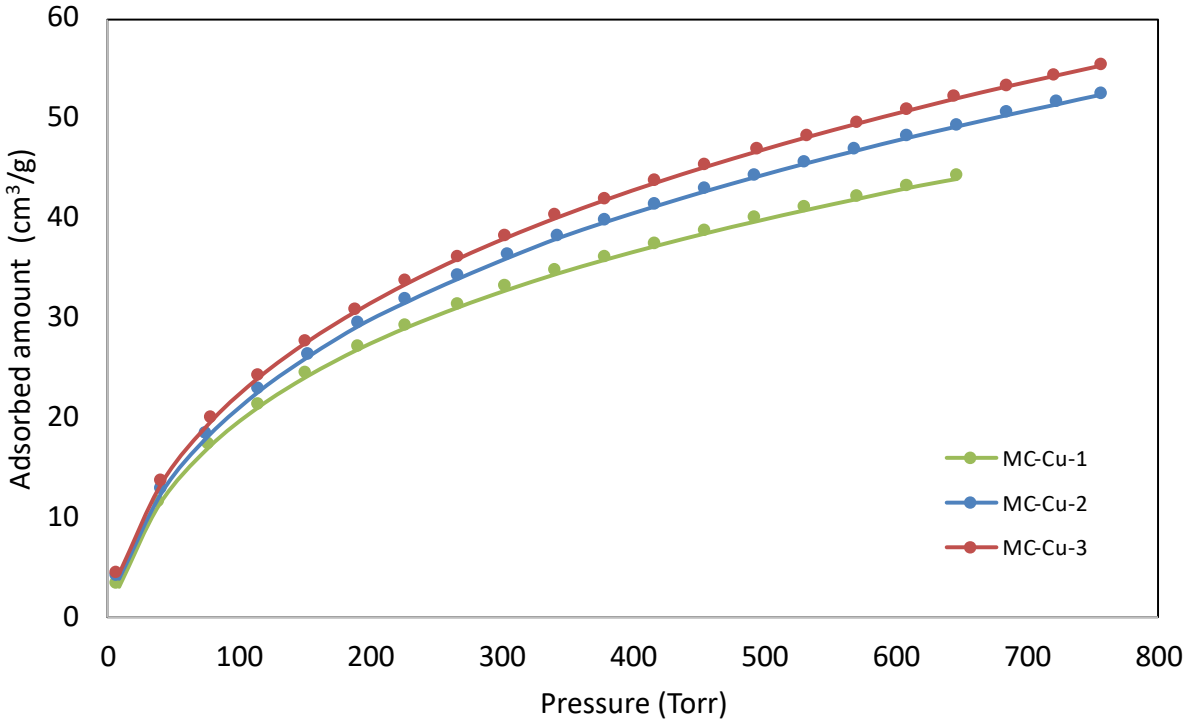

Figure S4. CO_2 adsorption isotherms at 273 K